RSC Advances

PAPER



Cite this: *RSC Adv.*, 2020, **10**, 37035

Received 12th August 2020
Accepted 30th September 2020

DOI: 10.1039/d0ra06962k

rsc.li/rsc-advances

# A fluorescent target-guided Paal–Knorr reaction†

Sachin B. Wagh, [a] Vladimir Maslivetc, [a] James J. La Clair *[b] and Alexander Kornienko *[a]

It has become increasingly apparent that high-diversity chemical reactions play a significant role in the discovery of bioactive small molecules. Here, we describe an expanse of this paradigm, combining a 'target-guided synthesis' concept with Paal–Knorr chemistry applied to the preparation of fluorescent ligands for human prostaglandin-endoperoxide synthase (COX-2).

Over the last decade, it has become clear that techniques such as protein-templated fragment ligation (PTFL)[1] or target-guided synthesis (TGS)[2] demonstrate the potential of biological targets to not only participate in the structure–activity relationship (SAR) analyses, but also engage in the synthetic effort. Other approaches have shown the use of proteins and cells as vehicles for lead isolation and selection,[3] therein identifying the possibility for methods enabling medicinal chemical studies to be conducted directly in the presence of a protein target.

To date, reversible chemical reactions catalyzed by protein pockets referred to as PTFL, include syntheses of hemiacetals, acetals, imines, hydrazones, oximes, *N*,*S*-acetals, boronate esters, disulfides, olefin cross-metathesis, and nitro-aldol additions.[4] Unfortunately, many of these reactions result in unstable ligands and often require additional operations to improve stability, such as the reduction of imines to amines with $NaBH_3CN$. Such added steps are undesirable, as amines could have different binding preferences than imine intermediates.[4c] Irreversible processes, commonly referred to as TGS, are primarily limited to addition of thiols to various electrophilic molecules[5a] and the click reaction,[5b] resulting in the formation of a thioether and triazole products, respectively. Clearly, adaptation of diverse irreversible reactions to TGS is required to enable the use of multifarious drug-friendly moieties.[6]

Pyrroles are a fundamental motif found in natural products and marketed drugs. It has been shown to deliver leads with anti-cancer, anti-inflammatory, anti-bacterial, anti-viral, anti-malarial, anti-convulsant, anti-hypertensive, anti-psychotic, anti-cholesterolimic and anti-nociceptive activities.[7] While many methods to synthesize pyrroles exist, the classical Paal–Knorr reaction,[8] involving the condensation of a primary amine with a 1,4-dicarbonyl, stands out due to the mild reaction conditions. This reaction has been well documented through a variety of synthetic applications, such as the commercial preparation of Lipitor.[9] In addition, the Paal–Knorr reaction is well known biologically.[10] It plays a role in human metabolism and has been implicated in the neurotoxicity of *n*-hexane.[10,11]

The mechanism of the Paal–Knorr reaction has been the subject of numerous investigations. The two main possibilities involve initial formation of enamine (**a** to **b**, Fig. 1) or hemiaminal (**a** to **d** Fig. 1). The calculation of potential energy surfaces using density functional theory suggests that the hemiaminal cyclization is the preferred reaction pathway.[12] This is further corroborated by real-time monitoring of the reaction between aniline and acetonylacetone using extractive electrospray ionization tandem mass spectrometry, where the dihydroxy compound (**d**, Fig. 1) was found to be a key intermediate on the reaction path.[13]

The Paal–Knorr reaction requires a mild acid, which is not surprising since each step in the reaction, namely initial attack of aniline **2** onto a carbonyl in **1** resulting in adduct **a**,

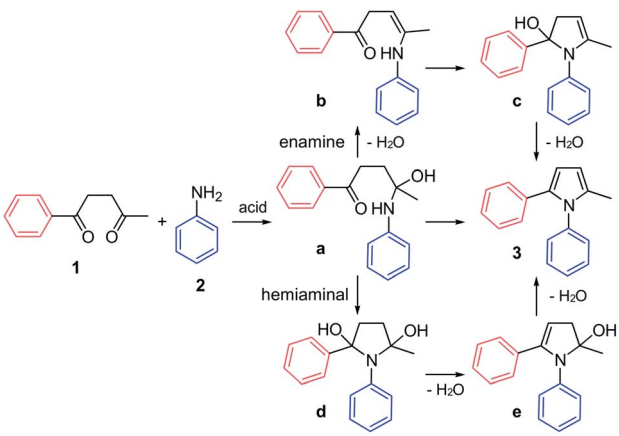


Fig. 1 Paal–Knorr synthesis of 1,2-diarylpyrroles **3** from diketone **1** and aniline **2** can proceed through two possible mechanistic pathways. Current experimental and theoretical results favor the hemiaminal (**a** to **e** *via* **d**) over the enamine (**a** to **c** *via* **b**) cyclization.

[a]*The Department of Chemistry and Biochemistry, Texas State University, San Marcos 78666, USA. E-mail: a_k76@txstate.edu*

[b]*Xenobe Research Institute, P. O. Box 3052, San Diego, USA. E-mail: i@xenobe.org*

† Electronic supplementary information (ESI) available: Experimental procedures and copies of spectral data. See DOI: 10.1039/d0ra06962k

cyclization of the latter to give **d**, and subsequent dehydrations leading ultimately to pyrroles **3**, could be accelerated by an acid catalyst. It is also tempting to propose that the Paal–Knorr reaction should proceed efficiently in presence of protein containing hydrogen bond donor residues provided that the substituents present in diketone **1** or aniline **2** and ultimately in pyrrole **3** could be accommodated at the binding site (see TOC graphic and Fig. S1†).

Moreover, when starting materials, intermediates and pyrrole products **3** are sterically and electronically compatible with the protein pocket, binding can bring reactants into close proximity thus promoting the transformation. This proposal is consistent with previous reports suggesting that the Paal–Knorr reaction could be accelerated in the presence of proteins.[14]

To reduce this proposal to practice, we adopted the transformation of aryl diketones **1a–m** and anilines **2a–m** to afford a panel of pyrroles **3aa–mm** as the focus of our study (Fig. 2a). We envisioned that this reaction would be catalyzed at the active site of COX-2, an important anti-inflammatory drug target.[15] This choice was based on the prior work describing diarylpyrroles as COX-2 selective inhibitors,[16] and the presence of multiple hydrogen-bond donor residues at its active site (H75, Q178, Y355, Y385, R499). It should also be noted that this enzyme has been previously reported to catalyze an "*in situ*" click reaction, resulting in the formation of triazole products.[17] This Paal–Knorr target-guided strategy is schematically illustrated in Fig. S1.†

We began by applying the Stetter reaction[16] utilizing methyl vinyl ketone to prepare 1,4-diketones **1a–m** from aldehydes **4a–m** (Fig. 2a). Here, we found that use of 20 mol% of thiazolium catalyst provides moderate to high yields of the diketone products in a highly reproducible fashion. Using diketone **1a** and aniline **2a** as a model, we then established screening to produce **3aa** in aqueous media. This began by developing conditions where **1a** and **2a** were sufficiently soluble in aqueous media. Using NMR methods, we found that 5% $CH_3CN$ in PBS pH 7.2 provided sufficient solubility (at 250 μM concentration for **1a** or **2a**) in PBS pH 7.2 without inducing undesired reactivity such as acetal formation (MeOH, EtOH) or oxidation (DMSO).

We then prepared pyrrole **3aa** synthetically (Fig. 2a) and found that it displayed blue fluorescence with $\lambda_{max}$ of 435 ± 10 nm (Fig. 2b). Using **3aa** as a guide, we developed a fluorescent screen to evaluate reactions containing 250 μM diketones **1a–m** with 250 μM anilines **2a–m** in PBS at pH 7.2 containing 5% $CH_3CN$. At this concentration, we screened the levels of COX-2 required to generate a fluorescent response. Fluorescence spectra were collected with $\lambda_{ex}$ at 260 nm and measuring the fluorescence from $\lambda_{em}$ at 280–600 nm from each well, compared to wells without COX-2. At concentrations above

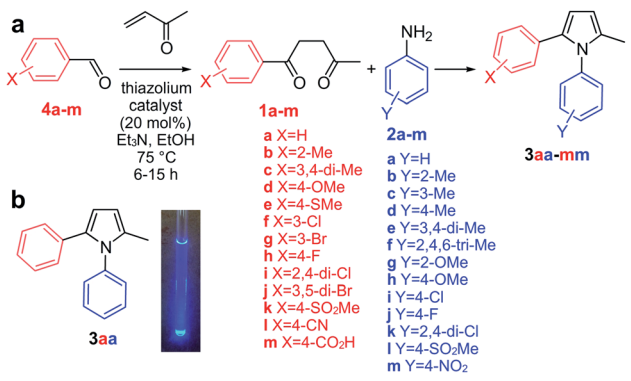


Fig. 2 Approach (a) A two-step process was used to prepare diketones **1a–m** from aldehydes **4a–m** using the Stetter reaction followed by Paal–Knorr condensation with anilines **2a–m** to afford pyrroles **3aa–mm**. (b) Fluorescence of **3aa** was visible upon excitation at 260–290 nm.

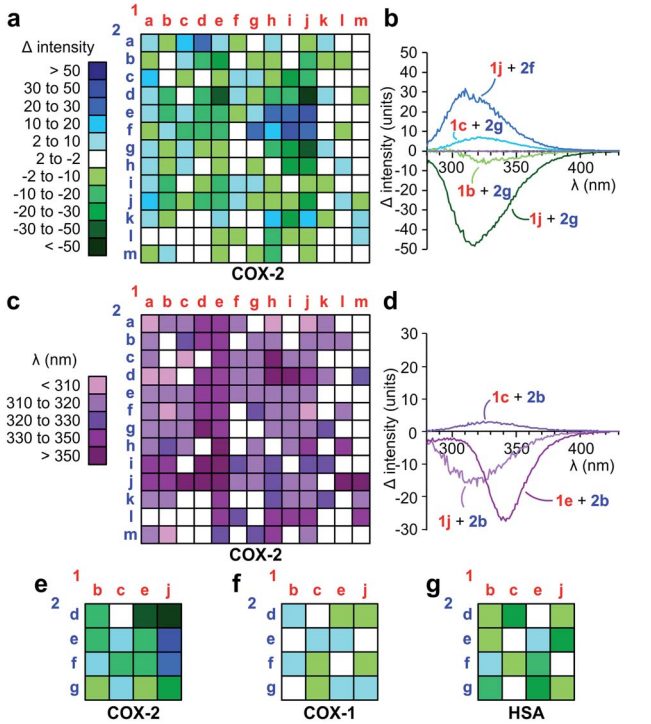


Fig. 3 Discovery of fluorescent ligands to COX-2. (a–d) Primary screen. Ketones **1a–m** (250 μM) were screened in an array against anilines **2a–m** (250 μM). The entire array was run in parallel for 2 h at 0 °C then 12 h at rt in presence (0.1 μM COX-2) or absence of COX-2. (a) Heat maps depicting difference in fluorescence between the reactions in the presence or absence of COX-2. Blue indicates a gain in fluorescence and green a loss in fluorescence. (b) Selected spectra used to generate the fluorescent intensity change heat maps. (c) In addition to intensity changes, different wavelengths of fluorescence were also observed from the spectra collected in the presence or absence of COX-2. Wavelengths are given from <310 nm (light purple) to >350 nM (dark purple). White indicates no fluorescence. (d) Selected spectra used to generate the spectral shift heat maps. We observed a change in the intensity and fluorescence maxima across the 169 reactions (13 × 13 reaction matrix). (e–g) Selectivity screen. A subset of the primary screen was subjected to selectivity analyses. Using identical conditions, we compared the fluorescence obtained in the presence of (e) 0.1 μM COX-2 to that generated in the presence of (f) 0.1 μM COX-1 and (g) 0.1 μM human serum albumin (HSA) in order to identify COX-2 selective products relative to COX-1 and general protein binders using HSA. Structures of all products in (e–g) are provided in Fig. S2.† Structures with the largest response ($\Delta$ > 20) in (a) are provided in Fig. S4.†

30 nM, a consistent trend was obtained over 3 repetitions and 0.1 μM COX-2 was set as the concentration for screening. Next, we evaluated the optimal reaction times. Time course fluorescent monitoring indicated that this process was ideally conducted by starting the reaction at 0 °C for 2 h and then warming it up to 23 °C over 1 h and incubating for ≥10 h at 23 °C.

Over 2 repetitions, we screened a 13 × 13 array of **1a–m** against **2a–m** (Fig. 3) using 250 μM **1a–m**, 250 μM **2a–m**, 0.1 μM COX-2 in PBS pH 7.2 containing 5% $CH_3CN$. Spectra for each reaction were compared against the corresponding reactions in the absence of COX-2 and the difference between these spectra were determined by subtracting the spectrum of the reaction without COX-2 from that with COX-2 (Fig. 3a). As shown in Fig. 3b, the presence of COX-2 either caused an increase (**1j** + **2f**) or reduction in fluorescence (**1j** + **2g**). This data was effectively displayed using a heat map based on the maximal change in the level of fluorescence (Fig. 3a). Interesting, the difference between the reactions with and without COX-2 also led to a change in wavelength (Fig. 3c). These shifts were observed from 300 nm to >350 nm as illustrated by maxima for **1e** + **2b**, **1c** + **2b** and **1j** + **2b** at $\lambda_{em}$ = 340, 325, and 318 nm, respectively (Fig. 3d).

Next, we challenged the Paal–Knorr approach to generate fluorescent pyrroles that would demonstrate selectivity for COX-2, the predominating cyclooxygenase at sites of inflammation, and not COX-1, constitutively expressed in the gastrointestinal tract.[18] For therapeutic use, the identification of fully-selective COX-2 inhibitors would reduce the effects on gastric mucosal prostaglandin synthesis observed with non-specific COX-2 targeting candidates.[19] While phylogenetically more primitive and very similar to COX-1,[15] COX-2 is distinguished by a smaller pocket within its active site. This pocket has played a key role in the selectivity of agents such as rofecoxib (Vioxx) or celecoxib (Celebrex).[20]

Using the data in Fig. 3a–d, we selected 16 reactions and prepared a 4 × 4 reaction array based on the highest differential in activity (dark green to dark blue, Fig. 3a) during our primary COX-2 screen. We found only modest changes in fluorescence in the presence of 0.1 μM COX-1 (Fig. 3f) or 0.1 μM HSA (Fig. 3g) when compared to 0.1 μM COX-2 (Fig. 3e). This selectivity was clearly evident in reactions conducted with **1j** (right column,

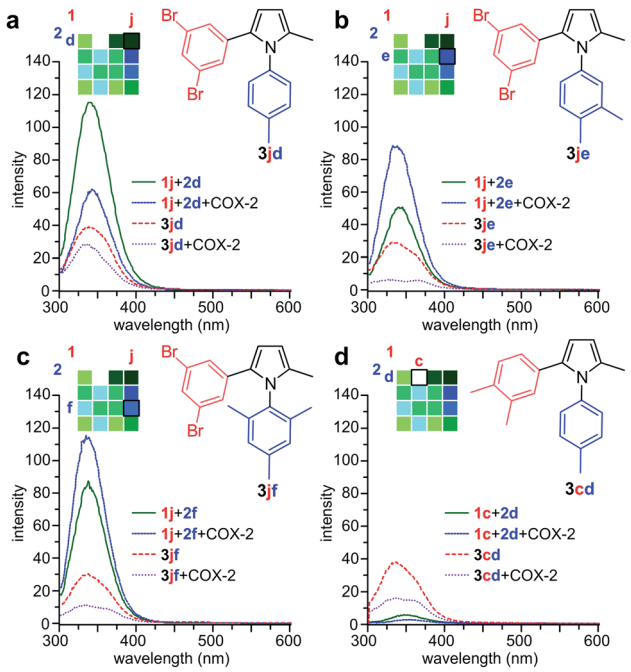


Fig. 4 Validation studies. (a) Comparison of the reaction of **1j** + **2d** in the absence (green) or presence (blue) of COX-2 against **3jd** in the absence (red) or presence (purple) of COX-2 (b) comparison of the reaction of **1j** + **2e** in the absence (green) or presence (blue) of COX-2 against **3je** in the absence (red) or presence (purple) of COX-2. (c) Comparison of the reaction of **1j** + **2f** in the absence (green) or presence (blue) of COX-2 against **3jf** in the absence (red) or presence (purple) of COX-2. (d) Comparison of the reaction of **1c** + **2d** in the absence (green) or presence (blue) of COX-2 against **3cd** in the absence (red) or presence (purple) of COX-2. Reactions were conducted using 250 μM **1c** or 250 μM **1j** and 250 μM **2d–f** using same conditions as in Fig. 3. Spectra were collected from reactions with 0.1 μM COX-2 or without COX-2. Spectra of the products were collected using 25 μM **3cd** or 25 μM **3jd–jf** with 0.2 μM COX-2 or without COX-2. A two-fold increase in COX-2 was used with **3jd–jf** to highlight the spectral changes.

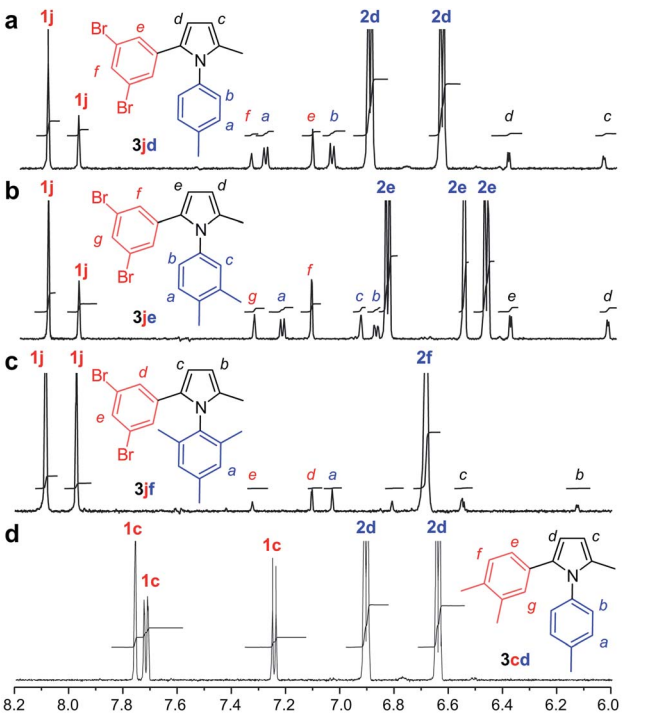


Fig. 5 Microscale NMR evaluation. (a) $^1$H NMR trace indicating the formation of **3jd** from the reaction of 250 μM **1j** with 1250 μM **2d** in the presence of 0.1 μM COX-2. (b) Comparable spectral data from the reaction of 250 μM **1j** with 1250 μM **2e** in the presence of 0.1 μM COX-2. (c) Comparable spectral data from the reaction of 250 μM **1j** with 1250 μM **2f** in the presence of 0.1 μM COX-2. (d) Comparable spectral data from the reaction of 250 μM **1c** with 1250 μM **2d** in the presence of 0.1 μM COX-2. These reactions were run at 10-fold increased scale compared to Fig. 3 (2 mL) to ensure accurate yield calculations. Five-fold excess of the aniline component was used in these reactions to encourage turnover. Additional spectra are provided in the ESI.†

Fig. 3e–g). Here, the 3,5-dibromo-substitution in diketone **1j** resulted in a positive gain in fluorescence when presented to **2e** and **2f** in the presence of COX-2 and a loss in fluorescence when presented to **2d** or **2g**.

We then evaluated if pyrrole formation would occur in the absence of COX-2 under the same set of conditions as used in the screens (Fig. 3). We scaled up the reactions of **1j** with **2d**, **2e**, and **2f**, so that we could chemically monitor them with TLC and $^1$H NMR analyses (Fig. S5†). The reactions were conducted using 250 μM of diketone and 250 μM aniline in 0.4 mL of PBS buffer containing 5% $CH_3CN$ at 23 °C. NMR and fluorescent monitoring (every 2.5 h for 15 h) indicated no conversion or fluorescence characteristic from pyrroles **3** during this period.

We then prepared samples of **3cd**, **3jd**, **3je**, and **3jf** synthetically (Fig. 2a) and compared the effect of COX-2 on their fluorescence relative to that observed in the reactions in Fig. 3. As shown in Fig. 4, we observed a decrease in fluorescence from reactions of **1j** with **2d** in the presence of COX-2, while the reactions between **1j** and **2e** or **2f**, resulted in a gain in fluorescence, when compared to reactions in absence of COX-2. In contrast, the incubation of synthetically prepared **3cd** and **3jd–jf** all resulted in a loss in fluorescence upon binding to COX-2. This fluorescence quench was observed after adding COX-2 to **3cd**, **3jd**, **3je**, or **3jf**. This indicates that while the levels of fluorescence will increase over the course of a reaction due to the formation of **3jd**, **3je**, **3jf** or **3cd** in the presence of COX-2, product binding to COX-2 would mask the fluorescent response.

Next, we turned to NMR for validation. As shown in Fig. 5a–c, we were able to observe the production of **3jd**, **3je** or **3jf** in the presence of COX-2 by $^1$H NMR with a 35 μL sample in a 1.7 mm capillary NMR tube. Using integration to compare relative concentrations of diketone **1j** to pyrroles **3jd–jf**, we determined that conversions for **3jd**, **3je** or **3jf** were 22%, 31%, and 5%, respectively. This corresponded to a turnover of 528, 740, 120 for **3jd**, **3je** or **3jf**, respectively, indicating that, while slow, this templated reaction did turnover. Additional studies indicated that celecoxib blocked this reaction (Fig. S6†), further suggesting that the reaction occurred within a pocket of COX-2 (Fig. 6). To further explore this selectivity, we applied our NMR methods to evaluate reactions that did not show a fluorescent response. As shown in Fig. 5d, we did not observe a reaction between **1c** and **2d** in the presence of COX-2, suggesting that a lack of fluorescent response suggests no Paal–Knorr reactivity.

Interestingly, the fluorescence quench appears to arise from the fact that binding to COX-2 requires a conformational regulation leading to a reduction of conjugated states when bound. This suggestion is in part supported by the X-ray crystal structure of celecoxib bound to COX-2 (Fig. 6a).[20] In order to explain why **3je** formed and **3cd** did not, we evaluated how these pyrroles occupy the celecoxib pocket in COX-2. We found that **3je** (Fig. 6b) can dock within the same bi-aryl pocket as celecoxib. Pyrrole **3cd** (Fig. 6c), which only contains methyl groups in these positions, would present additional steric requirements as well as lack the electronegativity required for interactions with COX-2.

Overall, we have shown that the Paal–Knorr reaction can be induced in the presence of COX-2 and utilized the combination of fluorescence screening and capillary NMR validation. Our work demonstrates a clear pipeline to implement this procedure for the development of fluorescent probes to a targeted protein (COX-2). Efforts are now underway to translate these materials into fluorescent probes for cellular applications as well as explore their pharmacological potential.

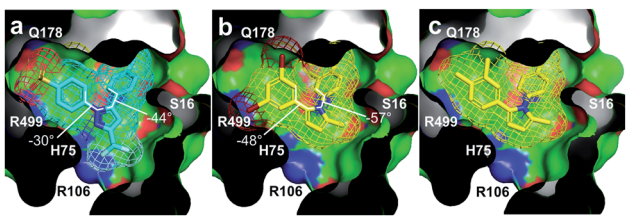


Fig. 6 Structural evaluation. (a) X-ray crystal structure (PDB ID 3LN1) depicting celecoxib (cyan) binding pocket in COX-2. The aromatic rings of celecoxib undergo deconjugative rotation, so that the aryl torsional angles[21] are $\varphi_1 = -30°$, $\varphi_2 = -44°$. (b) Image depicting **3je** (yellow) docked within the celecoxib binding pocket of COX-2 shown in (a). Here, the 3,5-dibromoaryl ring in **3je** could mimic the two S=O bonds within the sulphonamide in celecoxib (proximal to R499 and Q178). Energy minimized conformations of **3je** impose torsion angles of $\varphi_1 = -48°$, $\varphi_2 = -57°$ indicating that conformation access within the biaryl motifs of **3je** was comparable to that in celecoxib. (c) Image depicting **3cd** (yellow) docked within the celecoxib-binding pocket of COX-2. Expanded renderings in Fig. S3.†

## Conflicts of interest

There are no conflicts to declare.

## Acknowledgements

This work was supported by funding from the NIH under grant 1R21GM131717-01.

## Notes and references

1 (*a*) O. Seitz, *J. Pept. Sci.*, 2019, **25**, e3198; (*b*) M. Jaegle, E. L. Wong, C. Tauber, E. Nawrotzky, C. Arkona and J. Rademann, *Angew. Chem., Int. Ed.*, 2017, **56**, 7358.
2 X. Hu and R. Manetsch, *Chem. Soc. Rev.*, 2010, **39**, 1316.
3 P. Singh, K. Madhaiyan, M.-D. Duong-Thi, B. W. Dymock and S. Ohlson, *SLAS Discovery*, 2017, **22**, 440.
4 (*a*) L. Zhang, J. Dong, X. Xu and Q. Liu, *Chem. Rev.*, 2016, **116**, 287; (*b*) E. Burda and J. Rademann, *Nat. Commun.*, 2014, **5**, 1; (*c*) M. F. Schmidt, A. El-Dahshan, S. Keller and J. Rademann, *Angew. Chem., Int. Ed.*, 2009, **48**, 6346.
5 (*a*) E. Oueis, F. Nachon, C. Sabot and P.-Y. Renard, *Chem. Commun.*, 2014, **50**, 2043; (*b*) E. Oueis, C. Sabot and P.-Y. Renard, *Chem. Commun.*, 2015, **51**, 12158.
6 J. Ohkanda, *Chem. Rec.*, 2013, **13**, 561.
7 V. Bhardwaj, D. Gumber, V. Abbot, S. Dhiman and P. Sharma, *RSC Adv.*, 2015, **5**, 15233.
8 D. R. Dasari, J. J. La Clair and A. Kornienko, *Chembiochem*, 2017, **18**, 1792.

 

9 Y. V. Novozhilov, M. V. Dorogov, M. V. Blumina, A. V. Smirnov and M. Krasavin, *Chem. Cent. J.*, 2015, **9**, 7.
10 A. Kornienko and J. J. La Clair, *Nat. Prod. Rep.*, 2017, **34**, 1051.
11 J. W. Werner-Allen, J. F. DuMond, R. L. Levine and A. Bax, *Angew. Chem., Int. Ed.*, 2016, **55**, 7374.
12 B. Mothana and R. J. Boyd, *J. Mol. Struct.: THEOCHEM*, 2007, **811**, 97.
13 X. Zhang, M. Pei, D. Wu, S. Yang and Z. Le, *Sci. Rep.*, 2019, **9**, 19279.
14 N. Salehi and B. B. F. Mirjalili, *Iran. J. Catal.*, 2019, **9**, 185.
15 M. D. Ferrer, C. Busquets-Cortés, X. Capó, S. Tejada, J. A. Tur, A. Pons and A. Sureda, *Curr. Med. Chem.*, 2019, **26**, 3225.
16 I. K. Khanna, R. M. Weier, Y. Yu, P. W. Collins, J. M. Miyashiro, C. M. Koboldt, A. W. Veenhuizen, J. L. Currie, K. Seibert and P. C. Isakson, *J. Med. Chem.*, 1997, **40**, 1619.
17 A. Bhardwaj, J. Kaur, M. Wuest and F. Wuest, *Nat. Commun.*, 2017, **8**, 1.
18 J. A. Mitchell, N. S. Kirkby, B. Ahmetaj-Shala, P. Armstrong, M. Crescente, P. Ferreira, M. E. L. Pires, R. K. Vaja and T. D. Warner, *Pharmacol. Ther.*, 2020, **5**, 107624.
19 S. A. Schug, B. Parsons, C. Li and F. Xia, *J. Pain Res.*, 2017, **10**, 2451.
20 B. J. Orlando and M. G. Malkowski, *Acta Crystallogr., Sect. F: Struct. Biol. Commun.*, 2016, **72**, 772.
21 T. Egawa, K. Shinashi, T. Ueda, E. J. Ocola, W.-Y. Chiang and J. Laane, *J. Phys. Chem. A*, 2014, **118**, 1103.